Multiscale measurement of cardiac energetics

***Soyeon Goo,[1,3] *Toan Pham,[2] June-Chiew Han,[3] Poul Nielsen,[3,4] Andrew Taberner,[3,4] Anthony Hickey[2] and Denis Loiselle[1,3]**

Departments of [1]Physiology and [4]Engineering Science, [2]School of Biological Sciences, and [3]Auckland Bioengineering Institute, The University of Auckland, Auckland, New Zealand

Summary

1. We describe our laboratories' experimental methods for interrogating cardiac energetics – at the organ (whole-heart), tissue (trabecula) and perforated fibre (mitochondrial) levels.

2. In whole-heart and trabecula experiments, we focus on measuring pressure-volume (force-length) work and oxygen consumption (heat production) from which mechanical efficiency is derived. In both preparations, *i.e.*, across scales differing by three orders of magnitude, we find efficiency values of 10-15%. Mitochondrial experiments invoke a trio of titration protocols to yield information on oxygen consumption, ATP flux, membrane potential, electron leak and ROS production, the latter two of which index energy transfer inefficiencies.

Whole-heart energetics

Introduction

The measurement of cardiac energy expenditure has a long and illustrious history. As early as 1885, Yeo,[1] recording haemoglobin desaturation using spectroscopy, had estimated the rate of oxygen consumption of the frog heart, reporting its resting rate (with remarkable accuracy) to be about one-sixth of its total energy expenditure. In 1907, Barcroft & Dixon[2] utilized the Fick Principle to measure oxygen content of arterial and venous samples from isolated, blood-circulated, cross-perfused canine hearts, thereby achieving the first quantitative estimates of mammalian cardiac oxygen consumption. Evans[3] developed an ingenious method to ensure adequate oxygenation of isolated, non-supported hearts – using a heart-lung preparation, and accounting for trans-epicardial loss of oxygen. Three years later, Evans & Matsuoka[4] measured the work output of the heart and its associated metabolic cost. They calculated cardiac work using the Bernouilli expression for total fluid energy. Admitting that the direct measurement of pressure-volume work was beyond current technology, these workers nevertheless estimated peak cardiac efficiency to be 8-12%. The classical work of Starling & Visscher[5] demonstrated the metabolic consequence of the "Law of the Heart" and, germane to our focus, a peak mechanical efficiency of some 7%.

While technology has advanced since those pioneering experiments, the fundamental principle of measuring cardiac oxygen consumption ($\dot{V}O_2$) has not. It is still required to measure the amount of oxygen entering the coronary circulation *via* the coronary ostia (*a*), the amount leaving *via* the coronary sinus, right ventricle and pulmonary artery (*v*), and the rate of flow of perfusate ($\dot{V}$).

$$\dot{V}O_2 = \dot{V}(a - v) \qquad 1$$

This first approximation requires correction for oxygen exchange across the epicardial surface (see below).

Other indices of cardiac metabolism can be measured: the rate of production of CO_2 ($\dot{V}CO_2$), the rate of turnover of ATP ($\dot{A}TP$), or the rate of heat production ($\dot{Q}$) the latter of which is advantageous as it includes both aerobic and anaerobic sources, albeit with no ability to determine their relative contributions. In the following, we will examine and critically appraise the techniques of measuring $\dot{V}CO_2$, $\dot{Q}$ and $\dot{A}TP$, each of which we exploit in order to achieve multiscale measurement of cardiac energetics.

Energetics of the isolated working left-ventricle (whole-heart) preparation

Following isoflurane anaesthesia, thoracotamy and cardiectomy, an intact rat heart is Langendorff-perfused (*i.e.*, retrogradely, *via* the stump of the thoracic aorta,[6]) catheterized and instrumented, as follows. (i) A pressure-volume (P-V) catheter[7,8] is inserted into the left ventricle (LV) *via* one of the pulmonary veins and the left atrium (LA). (ii) An oxygen partial pressure (PO_2) electrode is advanced, *via* the aortic perfusion cannula, to reside just above the coronary ostia. This electrode measures coronary inflow PO_2 (P_aO_2). (iii) A second PO_2 electrode is inserted into the cannula draining the pulmonary artery, to determine coronary venous PO_2 (P_vO_2). To ensure oxygen saturation of inflow to the heart, in selected experiments (iv) a third PO_2 electrode is placed in the left atrial cannula. Temperature probes are placed in (iv) aortic, (v) pulmonary arterial, and (vi) left atrial PO_2 catheters. Flow probes reside in the (vii) aorta and (viii) pulmonary arteries to measure aortic ($\dot{V}_{aorta}$) and coronary venous ($\dot{V}_v$) flows, respectively. The rate of oxygen consumption by the working LV is given by:

$$\dot{V}O_2 = \dot{V}_v\sigma(P_aO_2 - P_vO_2) \qquad 2$$

where σ is the solubility of oxygen in isotonic saline (22.7 mL/L/atm at 37°C; Q_{10} = 0.83[9]). Finally, a unipolar

* Joint first authors

electrode (ix) is placed on the surface of the heart to pace it at a beat frequency (f) above the intrinsic heart rate. To produce a closed system, the remaining three pulmonary veins are ligated, as are the caudal and both cranial *vena cavae*. The heart is enclosed in a temperature-controlled, water-jacketed, glass chamber, the oxygen partial pressure of which (P_cO_2) can be varied.

Once fully instrumented and resident within the glass housing chamber, the (spontaneously beating) heart continues to be perfused in Langendorff mode until each measured variable reaches steady-state. At this point, perfusion is switched to working-heart mode[10] (paced at 4 Hz) for exploration of the metabolic cost of a range of mechanical demands. When this has been completed, perfusion is returned to Langendorff (*i.e.*, non-working) mode in order to estimate the resting (basal) rate of oxygen consumption. This requires perfusing the heart with some agent that induces cardiac arrest. We typically make use of either KCl (26 mM) or BDM (20 mM).

In all cases (whether Langendorff perfusion or working-heart mode, and whether beating or during arrest), the coronary circulation is perfused with HEPES-buffered Tyrode solution (pH-adjusted using Tris) in which the exogenous metabolic substrate is glucose (10 mM). It has been known since the work of Delcher & Shipp[11] that there is no difference in glucose uptake, lactate production, $^{14}CO_2$ production or glycogen levels in isolated, Tris-buffered rat hearts perfused with crystalloid solutions that have been equilibrated with CO_2 mixtures ranging from 2% to 20%. It is acknowledged, however, that perfusion of the isolated heart with a crystalloid solution reduces the concentration of both CrP and ATP *vis-à-vis* that of the blood-perfused heart *in situ*[12,13] and that prolonged perfusion may lead to tissue oedema.[14]

In working mode, the preload can be varied by changing the height of the pre-load chamber above the mid-level of the heart. The afterload is varied by changing the height of the aortic outflow catheter above the same reference point. The work of the heart can be measured in two independent ways: from the area of the pressure-volume loop displayed by the P-V catheter (Figure 1), and by the more conventional route: the product of aortic flow ($\dot{V}$) and mean afterload pressure ($\bar{P}_a$) divided by the heart rate.

Since the performance of pressure-volume work per beat and the oxygen consumption are measured simultaneously, the total efficiency of the heart can be quantified: $\varepsilon_{Total} = W/\Delta H_{total}$, where the denominator (the change of enthalpy) is given by the energetic equivalent of oxygen: 20.1 kJ/L (at standard temperature and pressure, duly corrected for ambient conditions). Subtraction of basal $\dot{V}O_2$ from the denominator of the preceding identity, yields the mechanical efficiency:

$$\varepsilon_{Mech} = W/(\Delta H_{total} - \Delta H_{basal}) \qquad 3$$

Representative data for such calculations are shown in Figure 1. Note that the calculated values of mechanical efficiency are both preload- and afterload-dependent. Note, further, that peak efficiency (approximately 13%) occurs at mid-range afterloads. Comparable behaviour has recently been demonstrated for isolated rat trabeculae.[15]

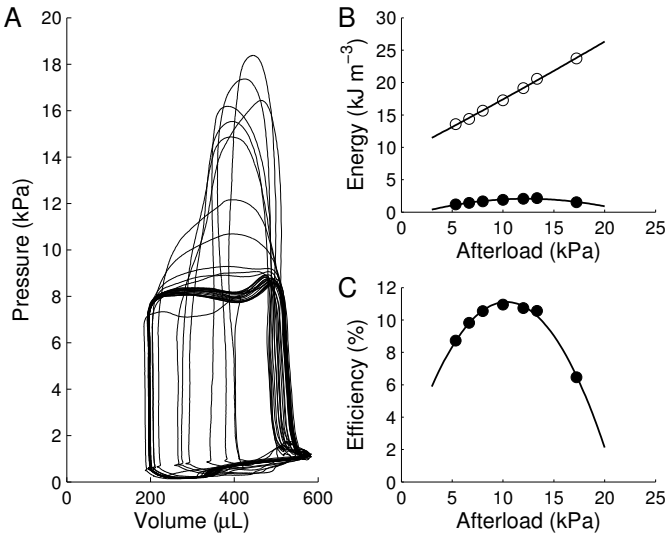

Figure 1. Energetics of the LV. A*: pressure-volume loops recorded using a conductance catheter in the left ventricle. Heavy black lines represent multiple steady-state beats at 1.3 kPa pre-load and 8 kPa afterload. Subsequently, afterload elevated stepwise to 18 kPa by progressive occlusion of the aortic outflow tract. For each loop, time increases counter-clockwise. Inability to achieve isovolumic contractions reflects parallel nature of coronary circulation flow, which increases with afterload.* ***B****: suprabasal energy expenditure (derived from rate of oxygen consumption, open symbols) and pressure-volume work (filled symbols).* ***C****: mechanical efficiency as a function of afterload at 1.3 kPa pre-load.*

Trans-epicardial flux of O_2

To quantify accurately either total or basal oxygen consumption, account must be taken of trans-epicardial oxygen exchange with the gaseous contents (room air) of the glass chamber housing the heart. Under our experimental conditions (perfusion with Tyrode solution equilibrated with 100% O_2), exchange is invariably a loss – thereby causing oxygen consumption to be overestimated. The resulting absolute error depends inversely on the surface area-to-volume ratio of the heart, so is greater the smaller the heart – both within and among species.[9,16,17] Furthermore, the relative error is greater the lower the metabolic rate, and therefore is relatively large for estimates of basal metabolism. The theoretical basis for correction, together with a practical method of its calculation, is given in Appendix I.

Tissue energetics

Our model of intact cardiac tissue is provided by rat trabeculae. Present in either ventricle,[15] trabeculae are minute, naturally-arising, axially-arranged, collections of

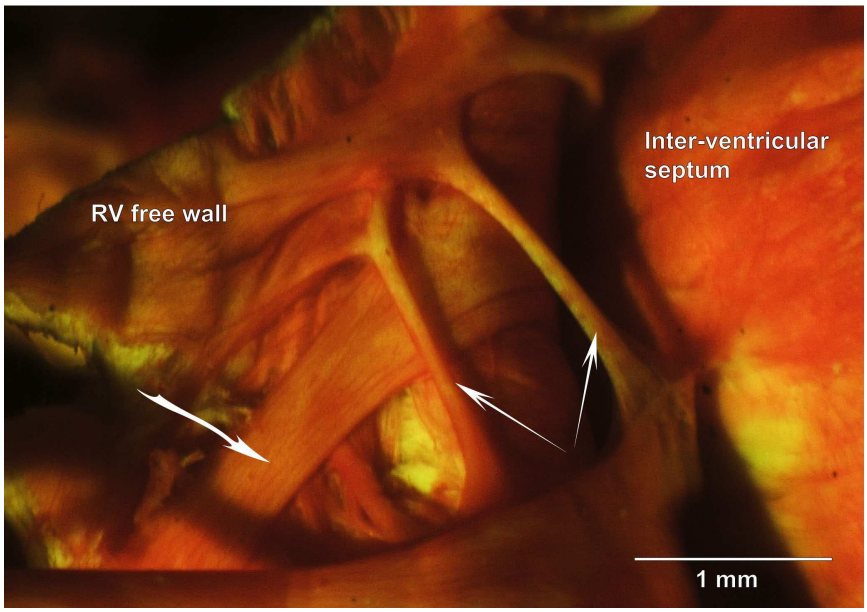

Figure 2. Photomicrograph of rat RV trabeculae. *Reproduced from Goo* et al. *(2009) Trabeculae carneae as models of the ventricular walls: implications for the delivery of oxygen. Journal of General Physiology, 134 (4): 339-350,[19] under the copyright privilege extended to authors by Rockerfeller Press.*

cardiac myocytes (Figure 2) of sufficiently small diameter to permit adequate diffusive oxygenation *in vitro*, even under high energy demand.[18] Whereas they may not completely replicate ventricular wall function[19] they have provided much insight into cardiac mechanics and energetics since the pioneering publication of ter Keurs *et al*.[20]

Over the past decade, we have developed flow-through microcalorimeters capable of measuring the minute quantities of heat produced by single trabeculae in response to isometric[21-24] and isotonic[25-27] contractions. Isotonic contractions permit quantitative analyses of force-length work-loops and, thus, comparisons between whole-heart and trabecula-derived estimates of mechanical efficiency. The principle of measuring trabecula heat production is straightforward. Using arrays of thermocouples, the increase in temperature of the superfusate as it flows along the length of the muscle is detected as a voltage-difference (ΔV) between downstream and upstream thermocouples. The product of ΔV, thermopile sensitivity, specific heat of the superfusate and flow rate yields the rate of heat production by the trabecula. Representative data from a LV trabecula, derived from simultaneous measurements of heat, force and displacement (Figure 3) predict that peak mechanical efficiency (12%) is comparable to that of the working heart (14%, Figure 1B) and not too dissimilar from the average value ($16.9 \pm 1.5\%$; N = 9) reported by Barclay & Wíden.[28]

Cardiac basal heat production ($\dot{Q}_{basal}$)

The basal metabolic rate, measured as heat production of the quiescent cardiac tissue, is notoriously difficult to determine. $\dot{Q}_{basal}$ varies inversely with heart size across species,[29] and values vary among laboratories, reflecting the use of different cardiac preparations, different measurement techniques and, especially, different methods of achieving cardiac arrest; independent estimates vary by more than an order of magnitude.[30] Our microcalorimetric technique presents an advantage: the resting state is achieved simply by turning off the electrical stimulator. However, microcalorimetry has not proved to be immune. Figure 4 shows perplexing behaviour; despite a great deal of scatter, the measurements show a clear decline of basal heat rate with increasing trabeculae length.

Given the results presented in Figure 4A, we developed a simple algebraic model to approximate the possible effect of heat production by the 'tethering tissues' at each end of the trabecula. These are short segments of ventricular wall or atrioventricular valvular tissue, which are placed into J-shaped hooks attached to quartz rods. These rods connect to a force-transducer at the down-stream end and a displacement motor at the upstream end within the measurement chamber. The algebraic model is presented in Appendix II. Its solution quantifies the contribution of an elevated value of $\dot{q}_{tether}$ (Figure 4B), which could, for example, reflect 'damaged ends' subsequent to dissection. But, from whatever source, if intensive heat rates and tissue volumes favour the 'end-tethers', then over-estimation of the true rate of cardiac basal metabolism would ensue. Such an error would be larger the shorter the trabecula. This issue is currently unresolved – a situation that dissuades us from reporting basal heat rates observed in the microcalorimeter.

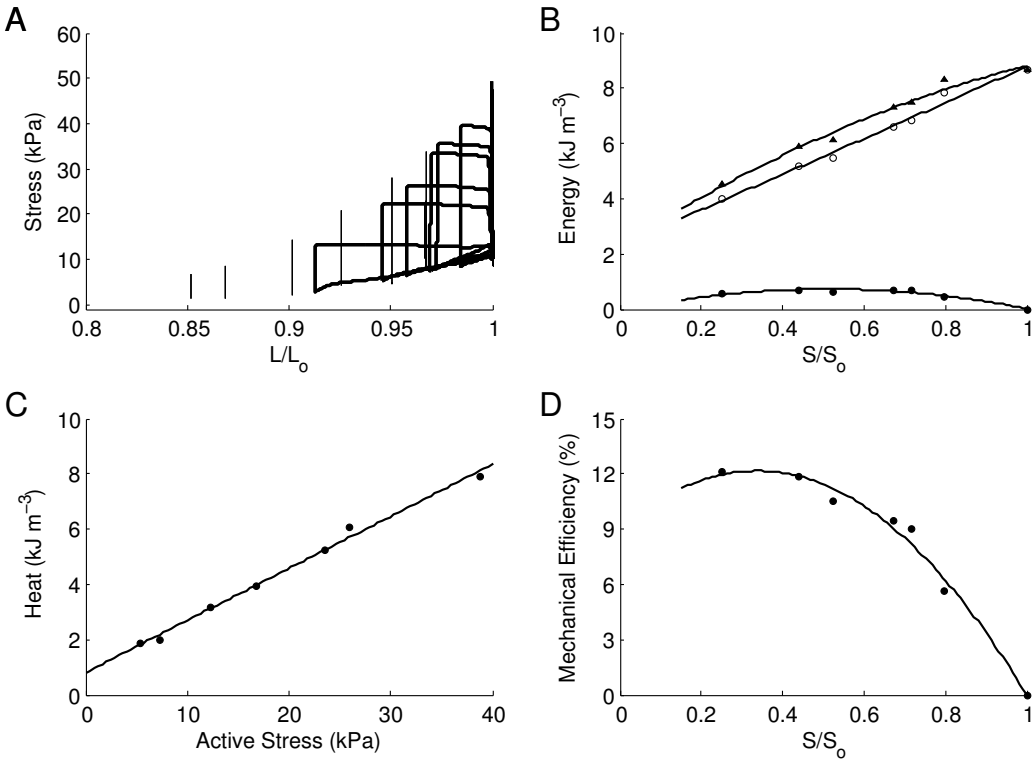

Figure 3. Mechanical and thermal performance of a rat LV trabecula stimulated at 3 Hz. ***A****: stress (force per cross-sectional area) produced during fixed-end (light vertical lines) and work-loop (heavy lines) contractions.* ***B****: work (lower-most trace), heat (middle trace) and change of enthalpy (heat + work, uppermost trace).* ***C****: Heat-stress relation from fixed-end contractions; same data as middle trace in B.* ***D****: Mechanical efficiency (work/enthalpy). S/S$_o$: relative afterload, where S = stress.*

Mitochondrial energetics

Background

Underlying the efficiency of cardiac contraction is the biochemical conversion of metabolic substrates into ATP through oxidative phosphorylation (OXP) mediated by mitochondria. Since Mitchell's[31] fundamental discovery of the underlying mechanisms of OXP, the efficiency of mitochondrial energetics has been debated. OXP efficiency is traditionally measured in terms of the P:O ratio (*i.e.* ATP formed per amount of molecular oxygen (O) reduced to water). While Mitchell noted that different substrates produce different P:O ratios, he estimated that P:O ratios were integers: 3 and 2, when electrons pass through Complex I (CI) and Complex II, respectively.[31] However, P:O ratios are no longer integers, with CI and CII substrates (*e.g.*, pyruvate, glutamate etc.) producing ratios of 2.8–2.5 and 1.8-1.6 respectively.[32] The discrepancies arose from the failure to account for the electrogenic import of substrates (*e.g.* P_i, ADP, glutamate, pyruvate), and experimental temperatures. At body temperature (*vis-à-vis* room temperature) mitochondrial membrane permeability to protons increases dramatically. This decreases the electrochemical gradient and increases the apparent proton leak.[33]

Experiments exploring P:O ratios have also been conducted with single substrates fuelling either, but not both, of CI and CII. While both complexes simultaneously contribute to the electron transport system (ETS) function *in vivo*, *in vitro* CI substrates do not stimulate CII, and subsequent succinate addition generally elevates overall oxygen flux[34] - by up to 95% in rat heart mitochondria.[35] Unlike CI, CII is non-proton-pumping and is coupled to OXP only at Complexes III and IV, and this lowers the P:O ratio of CII-mediated respiration relative to CI. Therefore one would expect the P:O ratio for the more life-like combined CI plus CII substrates to be lower and, hence, for OXP efficiency to be lower.

Another potential, albeit probably minor, source of inefficiency is the loss of electrons from the electron transport system (ETS) as the superoxide radical ($O_2^{\cdot-}$) formed from molecular oxygen at mitochondrial Complexes I and III.[36] *In vivo*, $O_2^{\cdot-}$ is normally enzymatically degraded by superoxide dismutase (SOD) to hydrogen peroxide (H_2O_2) or consumed by antioxidants and reduced to O_2 and H_2O by peroxidases and catalase.[37] Additional reactive species can also form, such as singlet oxygen and hydroxyl ions; collectively, these are called reactive oxygen species, or ROS.[38]

Mitochondrial ROS production appears to be greatest at high mitochondrial membrane potentials ($\Delta\Psi$)[36] which occurs when OXP is slowed or inhibited. The loss of

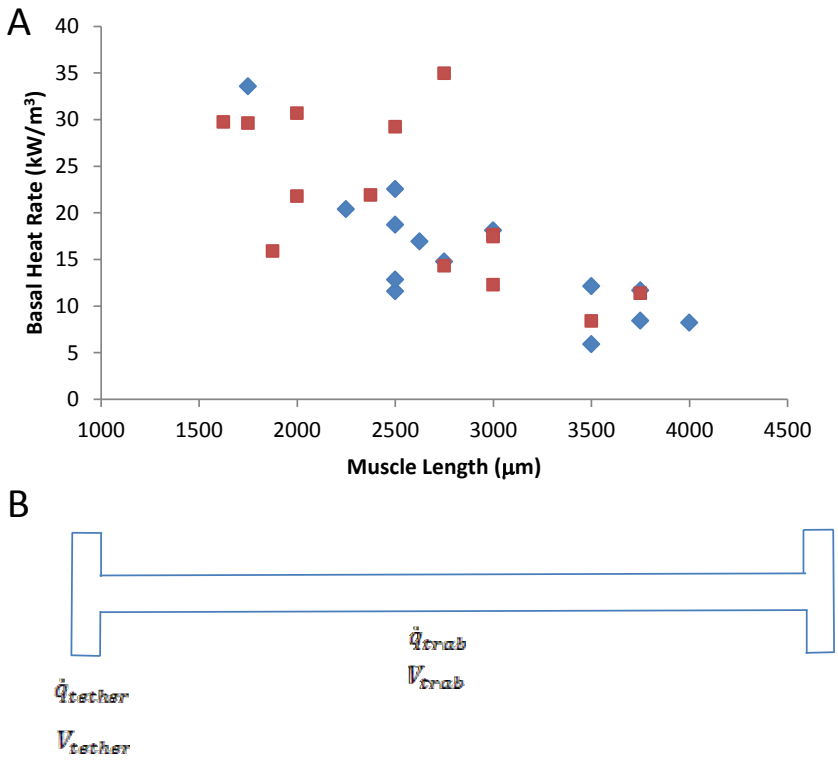

Figure 4. Cardiac basal metabolism. ***A:*** *observed length-dependence of rate of heat production of quiescent trabeculae; red squares: LV preparations, blue diamonds: RV preparations.* ***B:*** *Schematic diagram of an idealized trabecula with 'tethering tissue' at either end for positioning in the attachment hooks in the microcalorimeter.*

electrons through ROS has been reported to amount to 2-3% of the total oxygen consumed by mitochondria.[38] If real, this would be a measurable bioenergetic loss. However, ROS is rarely measured in different respiration states designed to mimic those occurring *in vivo*.[39] In the following, we present novel methodological approaches for the measurement of respirational flux simultaneously with real-time ATP production, $\Delta\Psi$ and net ROS production.

Experimental mitochondrial preparations

A choice of three distinct preparations is available for testing cardiac mitochondrial function: isolated mitochondria, permeabilized fibres and tissue homogenates. Whereas isolated mitochondria preparations have been widely used, isolation techniques provide poor yields (20-40%)[40] thereby requiring relatively large amounts of tissue (~500 mg to 1 g). Moreover, isolated mitochondria differ functionally from permeabilized fibres, showing higher ROS production and decreased respiration capacity.[41]

For the permeabilized fibre method, dilute saponin is used to perforate the sarcolemma by targeting cholesterol-rich membranes, while leaving mitochondrial membranes intact.[42] This maintains the mitochondrial cytoarchitecture within muscle fibres.[43] However, substrate diffusion, particularly for oxygen, ADP and ATP,[34] is restricted within permeabilized fibres.[44] Tissue homogenates provide a compromise between isolated mitochondria and permeabilized fibres. Like the latter, only a small (10-20 mg) sample is required so diffusion limitation is avoided.

Following cardiotectomy, the LV is cut into small pieces, and transferred into 1 ml cold HTK transplant buffer (Histidine-Trypophan-Ketoglutarate, Custodial®). Approximately 20 mg of LV tissue is weighed and transferred into 500 μL of ice-cold incubation assay medium (for details, refer to Veksler *et al.*, 1987[42]), homogenized for 15 s using a tissue homogenizer (Omni International, Georgia, USA) and used immediately.

High resolution respirometry

We use high-resolution oxygraphs (Oroboros O2K, Oroboros Instruments, Innsbruck, Austria) to measure oxygen consumption. Each has two 2-ml chambers with polarographic (Clark-type) oxygen sensors[45] and has additional amphoteric and voltimetric ports, which we use to couple purpose-built fluorimetric systems.[46] The real-time oxygen fluxes and changes in fluorophore signals are calculated using DatLab5 (Oroboros Instruments). Experiments are performed at 37 °C.

Mitochondrial respiration assays

We use substrate, un-coupler and inhibitor titration protocols to assess mitochondrial function in different respiration states: OXP, "Leak" respiration and uncoupled respiration, which measures ETS capacity.[34] The Leak state

Table 1: Titration protocols to test ATP synthesis capacities, mitochondrial membrane potential (Ψ) and ROS production. *Bleb: blebbistatin (50μM), Ou: ouabain (30μM), MgG: Magnesium Green (5μM), GMP: glutamate (10mM), malate (5mM), pyruvate (10mM), S: succinate (10mM), ADP: adenosine diphosphate (2.5mM), Oli: oligomycin (5μM), Saf: safranine-O (2μM), FCCP: carbonyl cyanide p-(trifluoromethoxy) phenol-hydrazone (0.5 – 1.5μM), AM: antimycin A (5μM), AMPR: amplex ultrared (5μM), HRP: horseradish peroxidase (2.5U), SOD: superoxide dismutase (25U), TMPD: N,N,N′,N′-tetramethyl-p-phenylenediamine (0.5mM), and Asc: ascorbate (2mM).*

Titration steps	Protocol-1 ATP assay	Protocol-2 Mitochondrial ΔΨ	Protocol-3 ROS assay
1	Bleb, Ou, MgG	2μM Saf	AMPR, HRP, SOD Calibrate with H_2O_2
2	Sample	Sample	Sample
3	GMP	GMP	GMP
4	S	S	S
5	ADP (Mg^{2+} free)	ADP	ADP
6	Run out of O_2	Oli	Oli
7	Oli	FCCP	FCCP
8		AM	AM
9		Calibrate with Saf	TMPD+Asc

is a measure of non-phosphorylating oxygen flux, determined either before addition of ADP or after the addition of OXP inhibitors (*e.g.*, oligomycin). Therefore Leak respiration reflects the capacity of the inner mitochondrial membranes to leak protons.[34,47] However, in the Leak state, the membrane potential is elevated and, in the presence of succinate, so is ROS production.[36]

OXP is initiated by addition of ADP in the presence of various substrates that fuel the ETS. In healthy mitochondria and permeabilized tissues and cells, ADP generally increases oxygen flux 7-10 fold as OXP commences and protons, flowing through the F_1/F_0 ATP synthase, partially depolarize the ΔΨ. The ratio of Leak flux to OXP flux theoretically provides an index of mitochondrial efficiency, where a high Leak relative to OXP indicates elevated, non-productive oxygen flux not associated with (decoupled from) ATP synthesis.[47] However, this approach is crude at best, since upon addition of ADP, ΔΨ will decline and potentially alter Leak, ROS and the driving force behind ATP synthesis. Moreover, if CI and CII substrates are added simultaneously, to stimulate mitochondria maximally, then the apparent Leak flux increases, yet the effects on ΔΨ remain unreported. How these events impact steady-state ATP synthesis rates and therefore, OXP efficiency, requires testing.

We present three protocols (Table 1) that explore mitochondrial efficiency. The first measures ATP production in normal and anoxic states, the second and third measure mitochondrial membrane potential and net ROS production, respectively.

Protocol 1: Measurement of ATP production rates in cardiac homogenates

Mitochondrial ATP production is rarely measured directly, being generally inferred from the change of oxygen flux following addition and depletion of a small amount of ADP. Whereas classically-derived P:O ratios provide estimates of efficiency, they can follow only apparent ADP consumption, thereby relying on extrapolation of plots and non-steady-state flux rates. Hence, the amount of ATP formed per O has been much debated.[32] Direct real-time measures of oxygen flux and steady-state rates of ATP synthesis would permit measures of OXP efficiency. We note that mitochondria can also become net consumers of ATP in anoxic states.[48] The relative cost of this is yet to be reported.

While ATP is abundant (5-10 mM) within cardiomyocytes,[49,50] ATP detection typically uses tedious end-point assays.[32] ATP can be coupled to luciferin-luciferase, but light is evanescent and luciferase consumes O_2.[51] ATP can also be measured through coupling glucose, hexokinase and NADPH,[52] however NADPH interacts with several dehydrogenases and oxidases.

The Mg^{2+}-binding capacity of ATP provides an alternative method for following ATP, since [Mg^{2+}] can be detected using the fluorescent probe Magnesium-Green (MgG, Molecular Probes).[48] While both ADP and ATP bind Mg^{2+}, ATP binds Mg^{2+} with a 9-fold greater affinity than does ADP, and ATP synthesized from ADP further binds Mg^{2+} ions and quenches MgG fluorescence. Quantification of ATP dynamics was previously performed using a complicated approach utilising binding constants of MgG for Mg^{2+}, and ATP and ADP for Mg^{2+}.[48] These values were either determined or sourced from other works, some of which were at different pH or temperatures to those that we use. Below, we outline a considerably simpler calibration method.

MgG is followed using excitation and emission wavelengths of 503 nm and 530 nm, respectively. Standard media are used and independent calibration experiments are first performed without sample. MgG (5 μM) is added to the chambers and Mg^{2+}-free ADP titrated stepwise (1.25,

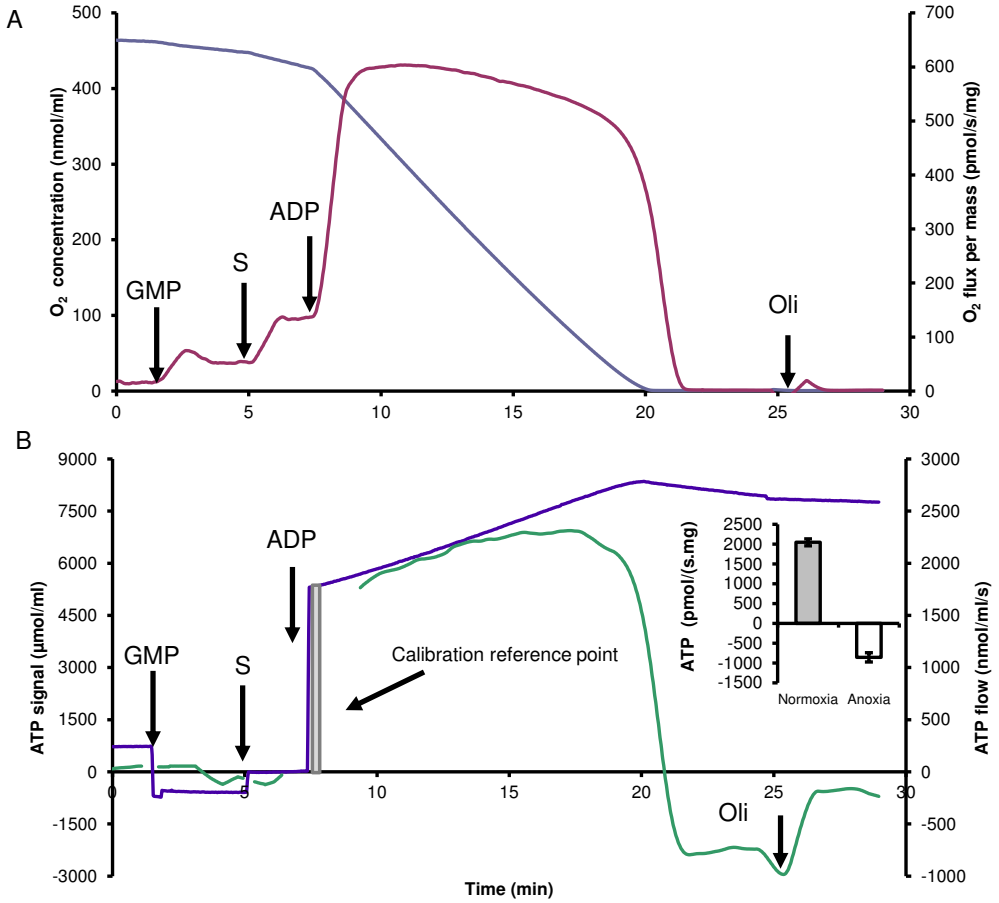

Figure 5. Simultaneous measurement of mitochondrial O_2 flux and ATP production. *The upper panel shows O_2 concentration (blue) and respiration flux (red). The lower panel shows MgG fluorescence (purple) and the time derivative of MgG fluorescence (green). The inset shows that, during anoxia, mitochondria can consume ATP at almost half the rate of normoxic ATP sysnthesis. For substrate abbreviations see Table 1. 'Calibration reference point' (vertical grey bars) denotes calibration step upon addition of Mg^{2+}-free ADP; brief segment of ATP signal deleted for clarity.*

2.5, 3.75, 5 and 6.25 mM). This process is repeated with Mg^{2+}-free ATP and ADP and ATP titration curves are constructed. The ratio of the signals between compounds is used to determine relative Mg^{2+} affinities of ADP and ATP; its value was found to be 2.15.

During an experiment, homogenate (2 mg, ~50 µL), MgG and all substrates and inhibitors (Table 1) are added except for Mg^{2+}-free ADP. Ouabain and blebbistatin are added to inhibit the Na^+/K^+ and myosin heavy-chain ATPases.[53] ADP (5 µmol) is used as the internal calibrant. Since the total adenylate pool remains constant, and changes of MgG fluorescence occur only due to changes in [ATP] relative to [ADP], the rate of ATP production (slope of the signal) can be multiplied by the fluorescence ratio of [ATP]/[ADP] (2.15) and the ATP output derived. ADP and ATP calibration curves are linear below 3.75 mM, and the total adenylate pool is below this concentration.

Measurement of ATP output (Figure 5) in anoxia informs the capacity for ATP hydrolysis. The addition of oligomycin (5 µM) returns the ATP production/hydrolysis rate to near zero, indicating that most of the consumption is mitochondrial. The minimal remaining signal accounts for the background degradation of ATP.

In Figure 5, leak in the presence of CI and CII substrates equates to 25.5 ± 1.3% (n = 12, ± sem). The mean steady-state P:O ratio equals 2.06 ± 0.10, which is lower than 2.34, the mean of P:O ratios derived using classical calculations for CI (2.87) and CII (1.8) substrates.[32] However, we note that previous work was conducted at 30°C, while our experiments were performed at 37°C. Using the steady-state P:O ratio, we accounted for the bond energy released on reduction of oxygen to water (−481 kJ/mol) and the energy captured by ATP (−57 kJ/mol under physiological conditions). By simple calculation of the energetic output relative to input: (2.06 × −57 kJ/mol / 0.5 × −481 J/mol), we derive an apparent efficiency of 48.8 ± 2.4% (n = 12 ± sem). This value is very similar to the optimal efficiencies predicted for CI-respiring heart mitochondria (~50% at 37°C) derived by Cairns *et al.*[54]) but is substantially less than that estimated by Barclay & Wíden[28] (~70%) from thermal measurements of post-exercise recovery metabolism made in isolated murine

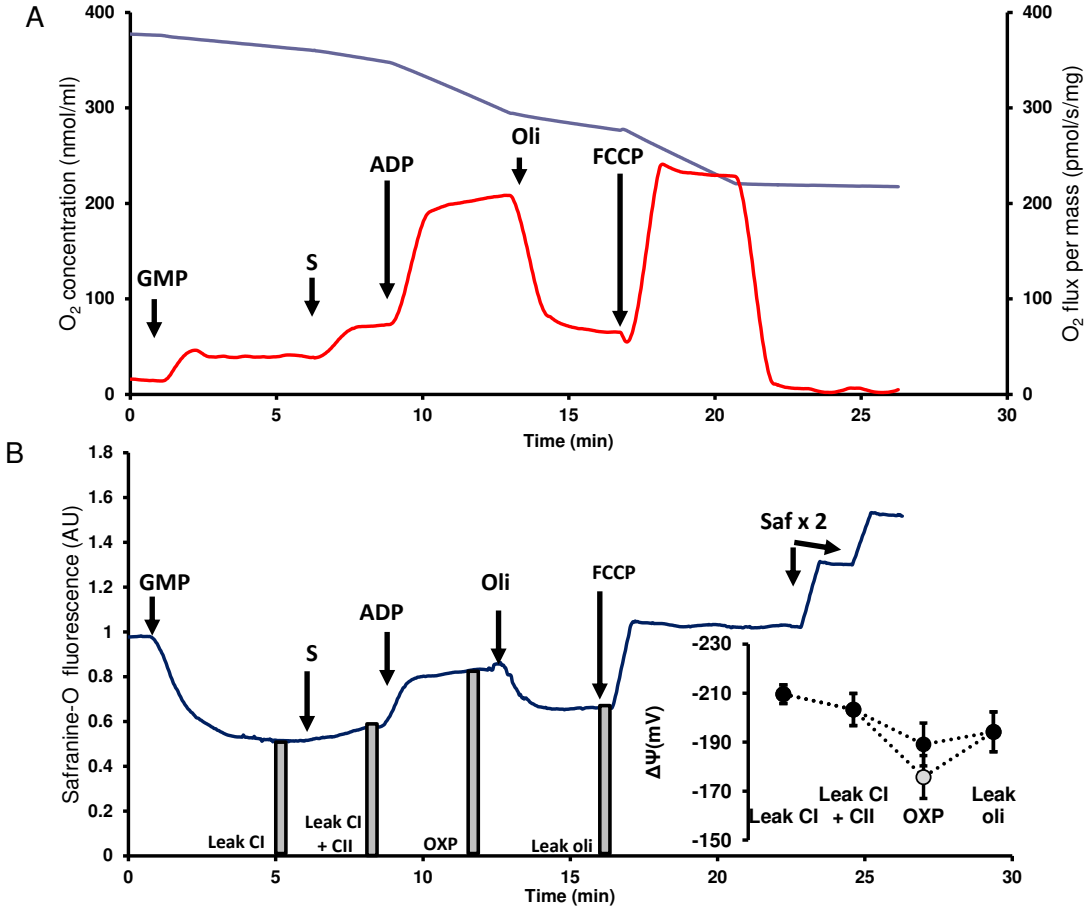

Figure 6. Assays of mitochondrial respiration and mitochondrial membrane potential. ***A:*** *O_2 concentration (blue) and oxygen flux (red), normalized by tissue mass.* ***B****: Safranine-O fluorescence (blue). Substrates and inhibitors added as per Table 1. Decreased fluorescence reflects quenching of safranine-O fluorescence, implying increasing ΔΨ. Additions of safranine-O (Saf) used to approximate the membrane potential (inset; black symbols) in each respiration state (vertical bars). Approximate values of ΔΨ for OXP calculated assuming dynamic shrinkage of mitochondrial matrix volume in OXP states (black circles) and fixed volume (grey circle) as traditionally reported.*

papillary muscles.

Protocol 2: assaying mitochondrial membrane potential (ΔΨ)

We use safranine-O to measure the mitochondrial membrane potential (ΔΨ) fluorimetrically, using excitation and emission wavelengths of 530 nm and 590 nm, respectively. Safranine-O is a lipophilic, cationic dye that distributes across the inner membrane of polarized mitochondria, and is quenched according to ΔΨ upon uptake and stacking within the matrix.[55,63] Safranine-O (2 μM) and substrate (Table 1) are added to each flourimeter chamber before adding 50 μL of homogenate. Once the safranine-O signal has stabilized, ADP (2.5 mM) is added to stimulate oxidative phosphorylation. The Leak rate from CI and CII is determined by addition of oligomycin (5 μM), followed by repeated titrations of FCCP (0.5 μM) to uncouple and depolarize mitochondria.[56] The addition of antimycin A (5 μM) inhibits Complex III and stops mitochondrial respiration. The addition of further safranine-O (1 μM) is used to calibrate the fluorescence signal (Figure 6).

While calibration of the safranine-O signal can be performed as stepwise KCl titrations in the presence of the K^+-ionophore valinomycin, this precludes the use of KCl in media. Since there is a linear relationship between safranine-O fluorescence and ΔΨ,[57] titration of safranine-O permits the estimation of ΔΨ (assuming that 40% of cardiomyocyte volume is mitochondrial,[58,59] and that mitochondrial matrix accounts for 63% of the mitochondrial volume).[60] ΔΨ is then estimated using the Nernst Equation:

$$\Delta\Psi = \frac{RT}{zF}\ln([Safranine]_{out}/[Safranine]_{in}) \qquad 4$$

where R is the universal gas constant, F is Faraday's constant, T is absolute temperature and z is the valence (+1) of safranine). Since mitochondrial matrix volume is dynamic and decreases by 40% in OXP states,[60] we calculate ΔΨ in OXP using both estimates of matrix volume

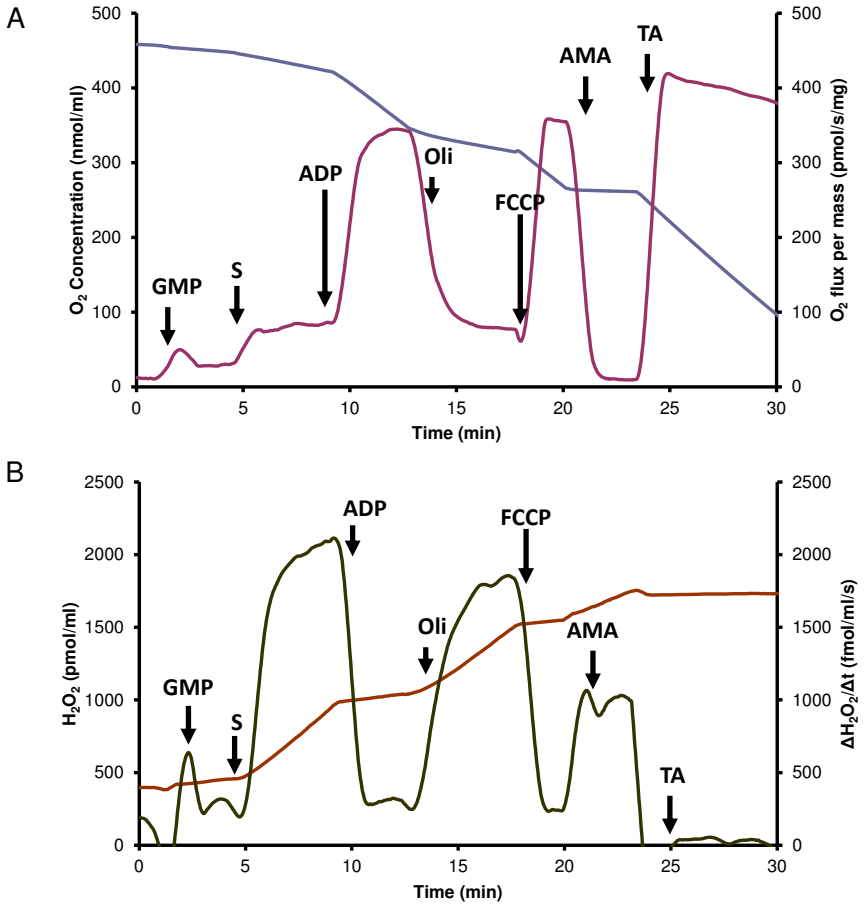

Figure 7. Mitochondrial respiration and ROS assays. *A: O_2 concentration (blue) and respiration flux (red) normalized by wet tissue mass (pmol/s/mg). B: Amplex Ultrarox Red (AMPR) (orange) and its time derivative (green). For substrate abbreviations, see Table 1.*

(see inset, Figure 6).

Our estimates of ΔΨ are within range of those estimated by standard means,[60] and while we show that ΔΨ is maximal with CI substrates alone, it decreased by approximately 6.3 mV upon addition of succinate (Figure 6). This is contrary to expectation, given that CII activation is expected to increase proton pumping further through CIII and CIV. Under a fixed mitochondrial volume, ADP decreased the apparent ΔΨ by 28 mV, whereas if a dynamic shrinking matrix volume were assumed, then ΔΨ would decrease by only 14 mV. While a dynamic matrix volume has previously been considered,[61] the phenomenon is universally ignored in calculations and, importantly, a high value of ΔΨ is thought to drive ROS production.

Protocol 3: assaying the net production of reactive oxygen species (ROS)

Following Hickey *et al.*,[46] net ROS production is measured simultaneously with respirational flux, using Amplex Ultrared (AMPR). The superoxide radical ($O_2^{\cdot-}$) released from mitochondria is reduced to H_2O_2 by both endogenous, and exogenously-supplied excess, superoxide dismutase (SOD). H_2O_2 is coupled to horseradish peroxidase (HRP) which, in turn, reacts with and AMPR to form Amplex Ultrox Red, a fluorescent product with 530 nm and 590 nm excitation and emission wavelengths, respectively.

Standard assay media are used and titrants added as per Table 1. AMPR, SOD and HRP are added to the fluorimeter chambers and followed as H_2O_2 (330 nM) to calibrate the ROS signal. Homogenate (2 mg) is again added into the chambers and allowed to equilibrate. Substrates (Table 1) are added and respiration and ROS signals followed (Figure 7).

As shown by the grey bars in Fig 8A, overall ROS production is 8- to 10-fold higher in the non-phosphorylating Leak state CI + CII relative to the CI Leak and OXP states. But when considering the consequences for efficiency, it is more meaningful to re-express these absolute values with respect to the uptake of oxygen, as in Figure 8B. Now it can be seen that ROS production accounts for only 0.02% of oxygen turnover in the more life-like (*i.e.*, putatively, maximally working) OXP flux state. Whereas the absence of ADP in Leak states probably doesn't ever occur *in vivo* (except, perhaps, during prolonged ischaemia), how a graded decrease in [ADP]

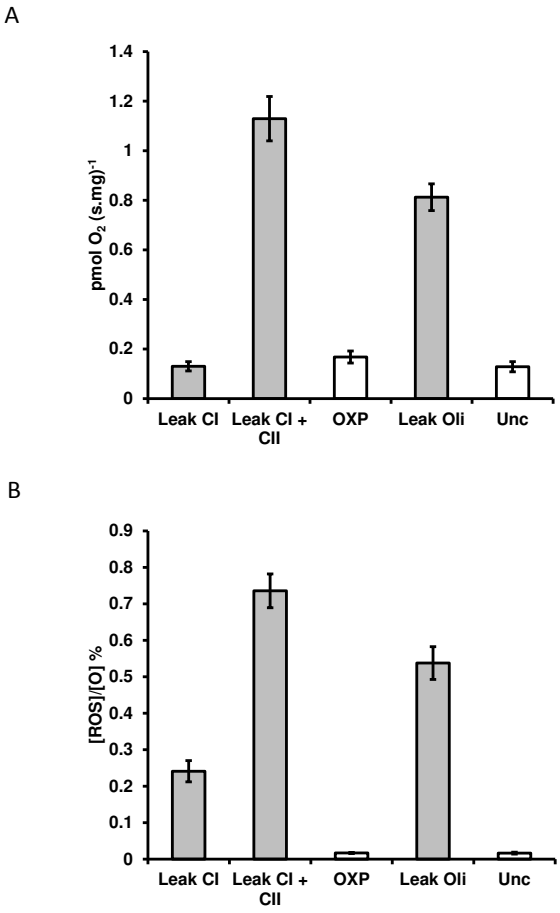

Figure 8. The production of reactive oxygen species (ROS) in rat left ventricle homogenate. *Grey bars represent non-phosphorylating Leak states measured in the presence of: complex I substrates ('Leak CI'), complex I and complex II substrates ('Leak CI + CII'), and oligomycin ('Leak Oli'). White bars represent phosphorylating states (OXP), the FCCP-uncoupled state (Unc), and following the addition of the Complex III inhibitor antimycin-A (AM).* ***A:*** *net ROS production;* ***B:*** *ROS production relative to uptake of molecular oxygen (ROS/O).*

within physiological ranges impacts ROS production is unknown and warrants exploration. The resulting knowledge would better clarify the role of ROS production and ETS efficiency within cardiomyocyte mitochondria under basal conditions and low-to-modest work-loads.

We note that different ROS probes are available, such as Amplex-Red, dihydroethidium (DHE) and its derivative MitoSOX, lucigenin, and dihydro-dichlorofluorescein. We have tested various probes; each provides different advantages and disadvantages. Overall, Amplex Ultrared proved to be the most stable, with minimal non-specific degradation, and it is very sensitive. MitoSOX, which is putatively specific to $O_2^{\cdot-}$ works well with isolated mitochondria and cells, but not in our system with permeabilized fibres. DHE may form a cation on oxidation to hydro-ethidium and, or ethidium. DHE lacks the lipophilic moiety of MitoSOX, and this may permit sequestration and quenching within mitochondria at high $\Delta\Psi$.[62] We have not tested the chemiluminescent Lucigenin; however, it proably requires a photomultiplier. Anecdotal information also indicates that Amplex ultrared will not work with liver homogenate as the probe is metabolized by endogenous oxidases.

Conclusion

Our ability to quantify mechanical efficiency at two distinct scales (whole-heart and isolated tissue) gives us confidence to conclude that the efficiency with which the heart performs external (pressure-volume) work is modest – in the vicinity of 10%, a value which is essentially unchanged from that first reported a century ago.[4]

The efficiency of the cardiac mitochondrial ETS is high with few electrons (0.02%) lost to the superoxide radical in OXP states. However, the efficiency of the OXP system is diminished by Leak respiration, which accounts for some 25% of OXP with CI and CII substrates. P:O ratios with these two substrates are 10% lower than those estimated using classical methods – a difference that may be attributable to our performance of assays at body temperature.

Appendix I: Determination of the true rate of oxygen consumption of an isolated, perfused heart in the presence of trans-epicardial flux of oxygen

The theoretical basis for correcting the measured rate of oxygen consumption of an isolated heart in the presence of trans-epicardial flux of oxygen has been given elsewhere.[9,64] Briefly, the *measured* rate of oxygen consumption ($\dot{V}_2^M$) is presumed to be the linear sum of two factors: the true rate of oxygen consumption of the heart ($\dot{V}_2^H$) and the rate of trans-epicardial oxygen leakage ($\dot{V}_2^L$)

$$\dot{V}_2^M = \dot{V}_2^H + \dot{V}_2^L \qquad \text{AI.1}$$

The true rate of oxygen uptake by the heart can be extracted from the measured rate by varying the rate of exchange flux of oxygen across the epicardial surface of the heart. In practice, this is done by vigorously flushing the glass chamber that houses the heart sequentially with either 0% or 100% O_2. The gradient for diffusive exchange is enhanced in the former situation and diminished in the latter. It is assumed that the diffusive oxygen conductance of the heart (D_H) is independent of PO_2 and is a unique property of each heart. We begin by defining v^* as the partial pressure of the coronary venous exudate that would prevail in the absence of diffusive epicardial flux and c as the experimentally-manipulated partial pressure of oxygen in the temperature-controlled glass chamber that houses the heart. This allows three independent equations to be written.

$$\dot{V}_1(a_1 - v_1^*) = \dot{V}_1(a_1 - v_1) - D_H(v_1^* - c_1) \qquad \text{AI.2}$$

$$\dot{V}_2(a_2 - v_2^*) = \dot{V}_2(a_2 - v_2) - D_H(v_2^* - c_2) \qquad \text{AI.3}$$

$$\dot{V}_1(a_1 - v_1^*) = \dot{V}_2(a_2 - v_2^*) \qquad \text{AI.4}$$

Equations AI.2 and AI.3 quantify the loss of oxygen across the epicardium under the two conditions of chamber PO_2. Equation AI.4 reflects the assumption that, during any metabolic steady-state, the true rate of oxygen consumption (given by the left-hand side of either Eq AI.2 or EqAI.3) is constant, independent of the partial pressure of oxygen in the chamber: $c_{1,2}$. Solution of this set of algebraic equations provides a unique numeric value for D_H, thereby allowing determination of either v_1^* or v_2^*

$$v_1^* = \frac{D_H c_1 - v_1 \dot{V}_1}{D_H - \dot{V}_1} \qquad \text{AI.5}$$

$$v_2^* = \frac{D_H c_2 - v_2 \dot{V}_2}{D_H - \dot{V}_2} \qquad \text{AI.6}$$

Substitution of this pair of equations into Equation AI.4 yields an expression that is quadratic in D_H:

$$\begin{aligned}&[\dot{V}_1(a_1 - c_1) - \dot{V}_2(a_2 - c_2)]D_H^2 \\ &+ [\dot{V}_2^2(a_2 - v_2) + V_1V_2[(a_2 - a_1) - (c_2 - c_1)] \\ &- \dot{V}_1^2(a_1 - v_1)]D_H \\ &+ [\dot{V}_1^2\dot{V}_2(a_1 - v_1) \quad - \dot{V}_1\dot{V}_2^2(a_1 - v_2)] = 0 \end{aligned} \qquad \text{AI.7}$$

Solution of Equation AI.7 yields:

$$D_H = \frac{-b \pm \sqrt{b^2 - 4ac}}{2a} \qquad \text{AI.8}$$

where

$$a = \dot{V}_1(a_1 - c_1) - \dot{V}_2(a_2 - c_2)$$

$$b = \dot{V}_2^2(a_2 - v_2) + \dot{V}_1\dot{V}_2[(a_2 - c_2) - (a_1 - c_1)] - \dot{V}_1^2(a_1 - v_1)$$

$$c = \dot{V}_1^2\dot{V}_2(a_1 - v_1) - \dot{V}_1\dot{V}_2^2(a_2 - v_2)$$

Substitution of the appropriate value of D_H into either Equation AI.2 or Equation AI.3 provides the desired estimate of $\dot{V}_2^H$.

Appendix II: Modelling the observed inverse dependence of cardiac basal heat production on trabecula Length

Figure 4 shows the disconcerting fact that the rates of basal metabolism measured in the microcalorimeter apparently depend inversely on the lengths of the trabeculae. Figure 4B shows an idealized trabecula whose end-tissues (which tether the specimen to the glass connecting rods *via* J-shaped platinum hooks, see text) may have differing rates of inherent heat production from that of the body of the trabecula: $\dot{q}_{tether}$ and $\dot{q}_{trab}$ respectively. They may also differ in volume: V_{tether} and V_{trab} respectively. This allows us to construct a simple algebraic model, as follows.

Let the *intensive* heat rate: $[\dot{q}] \equiv \left[\frac{kW}{m^3}\right]$

$\dot{Q}_{tether} = \dot{q}_{tether}V_{tether}$ where $\dot{Q}$ the *extensive* heat rate

$\dot{Q}_{trab} = \dot{q}_{trab}V_{trab}$

$\dot{Q}_{obs} = \dot{Q}_{tether} + \dot{Q}_{trab}$

where 'obs' means 'observed' (*i.e.* measured)

$\dot{Q}_{obs} = \dot{q}_{obs}\dot{V}_{trab}$, since $\dot{Q}_{obs}$ is normalized to V_{trab}. So

$$\dot{q}obs = \frac{\dot{q}_{trab}V_{trab} + \dot{q}_{tether}V_{tether}}{V_{trab}}$$

Thus

$$\dot{q}_{obs} = \dot{q}_{trab} + \dot{q}_{tether}\frac{V_{tether}}{V_{trab}}$$

and

$$\frac{\dot{q}_{obs}}{\dot{q}_{tether}} = 1 + \frac{\dot{q}_{tether}}{\dot{q}_{trab}} \frac{V_{tether}}{V_{trab}} = 1 + \frac{\dot{Q}_{tether}}{\dot{Q}_{trab}}$$

Thus it can be seen that if $\dot{Q}_{tether} > \dot{Q}_{trab}$ then the *measured* rate of heat production of a trabecula will exceed its *true* rate.

Acknowledgements

This work was funded by grants from the Health Research Council of New Zealand (11/585), the National Heart Foundation of New Zealand (*Small Project Grants* No 1428 and No 1529, and *Limited Budget Grant* No 1524) and the Maurice and Phyllis Paykel Trust (University of Auckland Project Number 3701355).

References

1. Yeo GF. An attempt to estimate the gaseous interchange of the frog's heart by means of the spectroscope. *J. Physiol.* 1885; **6**: 93-121.
2. Barcroft J, Dixon WE. The gaseous metabolism of the mammalian heart: Part 1. *J. Physiol.* 1907; **35**: 182-204.
3. Evans CL. The gaseous metabolism of the heart and lungs. *J. Physiol.* 1912; **45**: 213-34.
4. Evans CL, Matsuoka Y. The effect of various mechanical conditions on the gaseous metabolism and efficiency of the mammalian heart. *J. Physiol.* 1915; **49**: 378-405.
5. Starling EH, Visscher MB. The regulation of the energy output of the heart. *J. Physiol.* 1927; **62**: 243-61.
6. Langendorff O. Untersuchungen am überlebenden säugetierherzen. *Archiv für die gesamte Physiologie*. 1895; **61**: 291-332.
7. Baan J, Jong TTA, Kerknof PLM, Moene RJ, Van Dijk AD, Van Der Velde ET, *et al.* Continuous stroke volume and cardiac output from intra-ventricular dimensions obtained with impedance catheter. *Cardiovas Res*. 1981; **15**: 328-34.
8. Baan J, Van Der Velde ET, De Bruin HG, Smeenk GJ, Koops J, Van Dijk AD, *et al.* Continuous measurement of left ventricular volume in animals and humans by conductance catheter. *Circulation* 1984; **70**: 812-23.
9. Loiselle DS. Exchange of oxygen across the epicardial surface distorts estimates of myocardial oxygen consumption. *J. Gen. Physiol.* 1989; **94**: 567-90.
10. Neely JR, Liebermeister H, Battersby EJ, Morgan HE. Effect of pressure development on oxygen consumption by isolated rat heart. *Am. J. Physiol.* 1967; **212**: 804-14.
11. Delcher HK, Shipp JC. Effect of pH, pCo_2 and bicarbonate on metabolism of glucose by perfused rat heart. *Biochim. Biophys. Acta* 1966; **121**: 250-60.
12. Dobson JG, Schwab GE, Ross J, Mayer SE. Comparisons of the biochemical composition of four preparations of contracting cardiac muscle. *Am. J. Physiol.* 1974; **227**: 1452-7.
13. Headrick JP, Dobson GP, Williams JP, Mckirdy JC, Jordan L, Willis RJ. Bioenergetics and control of oxygen consumption in the in situ rat heart. *Am. J. Physiol.* 1994; **267**: H1074-84.
14. Van Dijk LC, Krams R, Sipkema P, Westerhof N. Changes in coronary pressure-flow relation after transition from blood to tyrode perfusion. *Am. J. Physiol.* 1988; **255**: H476-82.
15. Han J-C, Taberner AJ, Nielsen PMF, Loiselle DS. Interventricular comparison of the energetics of contraction of trabeculae carneae isolated from the rat heart. *J. Physiol.* 2013; **591**: 701-17.
16. Loiselle DS. The diffusive oxygen conductance of the heart. 1989, Muscle energetics, 315: 529-541, Alan. R. Liss, Inc. New York, Editors: Paul RJ, G Elzinga and K Yamada.
17. Loiselle DS, Van Beek JHGM, Mawson DA, Hunter PJ. The surface of the heart leaks oxygen. *NIPS* 1995; **10**: 129-33.
18. Han J-C, Taberner AJ, Kirton RS, Nielsen PMF, Archer R, Kim N, *et al.* Radius-dependent decline of performance in isolated cardiac muscle does not reflect inadequacy of diffusive oxygen supply. *Am. J. Physiol.* 2011; **300**: H1222-36.
19. Goo S, Joshi P, Sands G, Gerneke D, Taberner A, Dollie Q, *et al.* Trabeculae carneae as models of the ventricular walls: Implications for the delivery of oxygen. *J. Gen. Physiol.* 2009; **134**: 339-50.
20. Ter Keurs HE, Rijnsburger WH, Van Heuningen R, Nagelsmit MJ. Tension development and sarcomere length in rat cardiac traeculae. Evidence of length-dependent activation. *J. Physiol.* 1980; **46**: 191-7.
21. Taberner AJ, Hunter IW, Kirton RS, Nielsen PMF, Loiselle DS. Characterization of a flow-through microcalorimeter for measuring the heat production of cardiac trabeculae. *Rev Sci. Instrum.* 2005; **76**: 104902: 1-7.
22. Han J-C, Taberner AJ, Nielsen PMF, Kirton RS, Ward M-L, Loiselle DS. Energetics of stress production in isolated cardiac trabeculae from the rat. *Am. J. Physiol.* 2010; **299**: H1382-94.
23. Han J-C, Taberner AJ, Kirton RS, Nielsen PMF, Smith NP, Loiselle DS. A unique micromechanocalorimeter for simultaneous measurement of heat rate and force production of cardiac trabeculae carneae. *J. Appl. Physiol.* 2009; **107**: 946-51.
24. Han J-C, Tran K, Taberner AJ, Nickerson DP, Kirton RS, Nielsen PMF, *et al.* Myocardial twitch duration and the dependence of oxygen consumption on pressure-volume area: Experiments and modelling. *J. Physiol.* 2012; **590**: 4603-22.
25. Taberner AJ, Han J-C, Loiselle DS, Nielsen PMF. An innovative work-loop calorimeter for in vitro measurement of the mechanics and energetics of working cardiac trabeculae. *J. Appl. Physiol.* 2011; **111**: 1798-803.
26. Han J-C, Taberner AJ, Tran K, Nickerson DP, Nash MP, Nielsen PMF, *et al.* Relating components of

pressure-volume area in Suga's formulation of cardiac energetics to components of the stress-time integral *J. Appl. Physiol.* 2012; **113**: 988-95.
27. Han J-C, Taberner AJ, Tran K, Goo S, Nickerson DP, Nash MP, *et al.* Comparison of the Gibbs and Suga formulations of cardiac energetics: The demise of "isoefficiency". *J. Appl. Physiol.* 2012; **113**: 996-1003.
28. Barclay CJ, Widén C. Efficiency of cross-bridges and mitochondria in mouse cardiac muscle. In: Rassier D (ed). Muscle Biophysics: From Molecules to Cells, Advances in Experimental Medicine and Biology. Springer Science, New York. 2010.
29. Loiselle DS, Gibbs CL. Species differences in cardiac energetics. *Am. J. Physiol.* 1979; **237**: H90-8.
30. Gibbs CL, Loiselle DS. Cardiac basal metabolism. *Jpn. J. Physiol.* 2001; **51**: 399-426.
31. Mitchell P. Coupling of phosphorylation to electron and hydrogen transfer by a chemiosmotic type of mechansim. *Nature* 1961; **191**: 144-8.
32. Lee CP, Gu Q, Xiong Y, Mitchell RA, Ernster L. P/o ratios reassessed: Mitochondrial p/o ratios consistently exceed 1.5 with succinate and 2.5 with nad-linked substrates. *FASEB J*. 1996; **10**: 345-50.
33. Zukiene R, Nauciene Z, Ciapaite J, Mildaziene V. Acute temperature resistance threshold in heart mitochondria: Febrile temperature activates function but exceeding it collapses the membrane barrier. *Int. J. Hypertherm*. 2010; **26**: 56-66.
34. Gnaiger E. Capacity of oxidative phosphorylation in human skeletal muscle: New perspectives of mitochondrial physiology. *Int. J. Biochem. Cell Biol*. 2009; **41**: 1837-45.
35. Macdonald JR, Oellermann M, Rynbeck S, Chang G, Ruggerio K, Cooper GJS, *et al.* Transmural differences in respiratory capacity across the rat left ventricle in aging and diabetes: Mitochondrial dysfuncton begins in the myocardium. *Am. J. Physiol*. 2010; **300**: C246-55.
36. Murphy MP. How mitochondria produce reactive oxygen species. *Biochem. J.* 2009; **417**: 1-13.
37. Andreyev AY, Kushnareva YE, Starkov AA. Mitochondrial metabolism of reactive oxygen species. *Biochemistry (Moscow)*. 2005; **70**: 200-14.
38. Turrens JF. Mitochondrial formation of reactive oxygen species. *J.Physiol.* 2003; **552**; 335-344.
39. Hickey A, Renshaw G, Speers-Roesch B, Richards J, Wang Y, Farrell A, *et al.* A radical approach to beating hypoxia: Depressed free radical release from heart fibres of the hypoxia-tolerant epaulette shark (hemiscyllum ocellatum). *J. Comp. Physiol. B: Biochem, Systemic, Env. Physiol*. 2012; **182**: 91-100.
40. Lanza I, Nair K. Functional assessment of isolated mitochondria *in vitro*. *Meth. Enzymol*. 2009; **457**: 349-72.
41. Picard M, Taivassalo T, Ritchie D, Wright K, Thomas M, Romestaing C, *et al.* Mitochondrial structure and function are disrupted by standard isolation methods. *PLoS ONE*. 2011; **6**: e18317.
42. Veksler VI, Kuznetsov AV, Sharov VG, Kapelko VI, Saks VA. Mitochondrial respiratory parameters in cardiac tissue: A novel method of assessment by using saponin-skinned fibers. *Biochim. Biophys. Acta - Proteins & Proteomics*. 1987; **892**: 191-6.
43. Picard M, Taivassalo T, Gouspillou G, Hepple RT. Mitochondria: Isolation, structure and function. *J. Physiol*. 2011; **589**: 4413-21.
44. Vendelin M, Bovendeerd PHM, Arts T, Engelbrecht J, Van Campen DH. Cardiac mechanoenergetics replicated by cross-bridge model. *Ann. Biomed. Eng*. 2000; **28**: 629-40.
45. Gnaiger E. Polarographic oxygen sensors, the oxygraph and high-resolution respirometry to assess mitochondrial function. In: Dykens J and Will Y (eds). Mitochondrial Dysfunction in Drug-Induced Toxicity. John Wiley & Sons, Inc., Hoboken NJ. 2008; Ch. 12.
46. Hickey AJR, Renshaw GMC, Speers-Roesch B, Richards JG, Wang Y, Farrell AP, *et al.* A radical approach to beating hypoxia: Depressed free radical release from heart fibres of the hypoxia-tolerant epaulette shark (hemiscyllum ocellatum). *J. Comp. Physiol*. 2012; **182**: 91-100.
47. Pesta D, Gnaiger E. High-resolution respirometry: Oxphos protocols for human cells and permeabilized fibers from small biopsies of human muscle. In: Palmeira CM and AJ Moreno (eds). Mitochondrial Bioenergetics; Methods and Protocols, Methods in Molecular Biology. Humana Press Inc, New York. 2012.
48. Chinopoulos C, Vajda S, Csanády L, Mándi M, Mathe K, Adam-Vizi V. A novel kinetic assay of mitochondrial ATP-ADP exchange rate mediated by the ant. *Biophys. J.* 2009; **96**: 2490-2504.
49. Neubauer S. The failing heart — an engine out of fuel. *New England J. Med*. 2007; **356**: 1140-51.
50. Neubauer S, Horn M, Cramer M, Harre K, Newell JB, Peters W, *et al.* Myocardial phosphocreatine-to-ATP ratio is a predictor of mortality in patients with dilated cardiomyopathy. *Circulation* 1997; **96**: 2190-6.
51. Lyman GE, Devincenzo JP. Determination of picogram amounts of ATP using the luciferin-luciferase enzyme system. *Anal. Biochem*. 1967; **21**: 435-43.
52. Manfredi G, Yang L, Gajewski CD, Mattiazzi M. Measurements of ATP in mammalian cells. *Method Enzymol*. 2002; **26**: 317-26.
53. Kovács M, Tóth J, Hetényi C, Málnási-Csizmadia A, Sellers JR. Mechanism of blebbistatin inhibition of myosin II. *J. Biol. Chem.* 2004; **279**: 35557-63.
54. Cairns CB, Walther J, Harken AH, Banerjee A. Mitochondrial oxidative phosphorylation thermodynamic efficiencies reflect physiological organ roles. *Am. J. Physiol*. 1998; **274**: R1376-83.
55. Zanotti A, Azzone GF. Safranine as membrane potential probe in rat liver mitochondria. *Arch. Biochem. Biophys.* 1980; **201**: 255-65.

56. Hickey AJ, Chai CC, Choong SY, Costa SDF, Skea GL, Phillips AR, *et al.* Impaired ATP turnover and ADP supply depress cardiac mitochondrial respiration and elevate superoxide in nonfailing spontaneously hypertensive rat hearts. *Am. J. Physiol*. 2009; **297**: C766-74.
57. Figueira TR, Melo DR, Vercesi AE, Castilho RF. Safranine as a fluorescent probe for the evaluation of mitochondrial membrane potential in isolated organelles and permeabilized cells. *Meth. Mol. Biol*. 2012; **810**: 103-17.
58. Barth E, Stämmler G, Speiser B, Schaper J. Ultrastructural quantitation of mitochondria and myofilaments in cardiac muscle from 10 different animal species including man. *J. Mol. Cell. Cardiol.* 1992; **24**: 669-81.
59. Macdonald JR, Oellermann M, Rynbeck S, Chang G, Ruggiero K, Cooper GJS, *et al.* Transmural differences in respiratory capacity across the rat left ventricle in health, aging, and streptozotocin-induced diabetes mellitus: Evidence that mitochondrial dysfunction begins in the subepicardium. *Am. J. Physiol*. 2011; **300**: C246-55.
60. Bazil JN, Buzzard GT, Rundell AE. Modeling mitochondrial bioenergetics with integrated volume dynamics. *PLoS Comp. Biol*. 2010; **6**: e1000632.
61. Petronilli V, Pietrobon D, Zoratti M, Azzone GF. Free energy coupling between H^+-generating and H^+-consuming pumps: Ratio between output and input forces. *Eur. J. Biochem.* 1985; **155**: 423-31.
62. Näpänkangas JP, Liimatta EV, Joensuu P, Bergmann U, Ylitalo K, Hassinen IE. Superoxide production during ischemia–reperfusion in the perfused rat heart: A comparison of two methods of measurement. *J. Mol. Cell. Cardiol.* 2012; **53**: 906-15.
63. Akerman KE, Wikstrom MK. Safranine as a probe of the mitochondrial membrane potential. *FEBS Lett*. 1976; **68**: 191-7.
64. Loiselle DS, Van Beek JHGM, Westerhof N. Diffusion of oxygen across the surface of the isolated perfused guinea-pig heart is not negligible. 1990; *J. Physiol*. 420: 133P (Abstract)

Received 7 February 2013, in revised form 12 April 2013.
Accepted 18 April 2013.

Author for correspondence:

Denis Loiselle
Department of Physiology
University of Auckland,
Auckland, New Zealand

Tel: +64 9 373 7599 x86202
Fax: +64 9 373 7499
E-mail: ds.loiselle@auckland.ac.nz;